AIMS Materials Science, 10(3): 453–464.
DOI: 10.3934/matersci.2023025
Received: 11 March 2023
Revised: 19 May 2023
Accepted: 04 June 2023
Published: 16 June 2023

http://www.aimspress.com/journal/Materials

Research article

Welding on C67 steel grade sheet: Influence of the parameters and post welding heat treatment

Utpal K. Dhar[1], Md. Farabi Rahman[2,*], Mustafa Oguzhan Ayanoglu[1] and Ahammad Abdullah[1]

[1] Department of Ocean and Mechanical Engineering, Florida Atlantic University, Boca Raton, Florida, USA
[2] Department of Material Science and Chemical Engineering, Stony Brook University, NY, USA

*** Correspondence:** Email: mdfarabi.rahman@stonybrook.edu.

Abstract: In batch operation, most industries require engineers to maintain low hardness on the welded parts, particularly for low carbon steel. This article focuses on tungsten inert gas (TIG) welding performed on 0.90 mm of a C67 grade sheet by varying different welding parameters such as current, velocity, and temperature. Samples were collected from the tool side, mid-wall, and operator side for metallographic and micro-hardness examinations considering various parameters. Without post welding heat treatment (PWHT), the welded parts were quenched at room temperature, while with PWHT the welded parts were kept at 710 ℃ for 99 s after welding, and subsequently, the samples were cooled slowly by air at ambient temperature. An increase in hardness was registered in either the fusion zone or melted zone, with decrements in the heat affected zone (HAZ) for both procedures. When the the welding was performed without PWHT, a martensitic and bainitic microstructure was noticed in the melting zone (MZ) and HAZ, respectively. In contrast, a bainitic microstructure was observed in either the melting or heat affected zone in the welding with PWHT. Metallographic images revealed crack propagation when welding was performed without PWHT. A larger HAZ was noted in the welding sample with PWHT, and hardness was also relatively lower compared the samples without PWHT. There was no significant difference in hardness among the samples taken from tool side, mid-wall, and operator side for both procedures. Finally, the lowest microhardness (265 HV) was found in the MZ when the welding was carried out with PWHT employing a 90 A current and 10 mm/s velocity.

Keywords: C67 steel; TIG welding; Post welding heat treatment (PWHT); microstructure; hardness

1. Introduction

In recent years, researchers have focused more on investigating the strength and modulus of composite materials [1,2]. Because composite materials have some limitations for use in commercial activity, particularly with tungsten inert gas (TIG) welding, low or high carbon steel exhibits excellent compatibility with TIG welding [3–10]. TIG welding is widely used with stainless steel and nonferrous materials, such as aluminum and magnesium, but can be applied to nearly all metals, with notable exceptions such as lead and zinc. Its applications involving carbon steels are limited, not because of process restrictions, but because of the existence of more economical steel welding techniques, such as gas metal arc welding and shielded metal arc welding. For ferrous metals, TIG welding is frequently performed due to its simplicity and excellent final results [11,12]. In TIG welding, the weld area is protected from atmospheric contamination by utilizing a shielding gas, such as Argon. Sometimes, a filler metal is used, though for some welds, known as autogenous welds, a filler metal is not required. A constant current welding power supply produces energy, which is conducted across the arc through a column of highly ionized gas and metal vapors. According to Li et al. [13], the variation of welding parameters affects the temperature distribution and weld pools due to the oxygen concentration. Furthermore, Zmitrowicz et al. [14] concluded that alternating welding parameters can influence hardness, microstructure, and welding geometry. In the melting zone (MZ), the welding speed proportionally increases with the microhardness [15,16]. Li et al. [15] concluded that the fusion zone has a higher strength with decreased elongation compared with the base material. According to them, the uniform hardness value is found in the welded joint when fast cooling is performed. Post welding heat treatment (PWHT) is a common technology that has been widely used after TIG welding is executed [17–22]. Although it is very difficult to measure the grain size of low carbon steel, PWHT increases the grain size on the melting zone [12,23–25]. The main purpose of PWHT is to bring unform hardness in the base material (BM), heat affected zone (HAZ), and MZ [26]. According to Krółicka et al. [19], a bainite microstructure is found on 55Si7 grade steel when TIG welding is conducted after PWHT. Lan et al. [27] exhibited a bainitic microstructure in the HAZ when the welding was executed on low carbon steel and the presence of an inclusion did not affect the refinement of the HAZ microstructure. Although many experiments were performed for various materials using TIG welding to improve the strength, our study correlates the microstructure with the hardness for different welded zone [28–33] for both types of welding. Welding technology, such as metal inert gas (MIG) welding, is not suitable for a flat sheet with low thickness (<3 mm) due to technical issues. Usually, TIG welding is performed on low carbon flat sheets because of its cheaper cost, distinct property, and availability in the market [33]. Current research studies aim to enhance the mechanical properties of welded metals, as well as to develop new techniques and optimize welding parameters in order to establish structure property relationships [34–36]. According to Kumar et al. [37], a thick cross-section can be welded as a single pass by TIG welding, and it substantially improves the welded joint by refining the welding penetration depth at a lower heat input. In this study, a TIG welding method is adopted on C67 grade materials by diversifying the welding parameters to compare the difference between welding with and without PWHT.

2. Materials and methods

We investigated a standard C67 grade steel sheet material with 0.90mm thickness with the chemical composition and mechanical properties shown in Table 1.

Table 1. Chemical composition used on for butt joint.

Element	C	Mn	Cr	Si	P	S	Al	V	Pb
% Weight	0.674	0.64	0.032	0.226	0.010	0.002	0.009	0.003	0.001

The material has an ultimate tensile strength and yield strength of 587 and 490 N/mm^2, respectively, with 21% elongation. A butt joint was made with the same C67 steel with single pass and without adding any other material. In this experiment, no preheating was performed prior to welding and the welding samples were examined with and without PWHT for the same material and thickness. The welded part was drastically cooled at room temperature without PWHT, kept to 710 ℃ for 99 s, then was slowly cooled at ambient temperature. We selected this temperature and time which was optimized during welding experiments. The different parameters such as current, velocity, and phase used to weld the sheet metal are listed in Table 2.

Table 2. Welding parameters employed in this study.

Input Voltage Power(V)	Current(A)	Velocity(mm/s)
380	65	4
380	100	7
380	90	6
380	120	15
380	33	6
380	90	10

The samples were characterized at the tool side, mid-wall, and operator side, where two types of characterizations (morphological and mechanical) were carried out to understand the structure property relationship.

2.1. Metallographic examination

The structural properties were investigated using a Nikon CFI60 Infinity Optical System. Three transverse specimens were selected from the machine side, mid-wall, and operator side for the C67 material. An abrasive cut-off blade with lubrication was used to cut the different sections of the sample, followed by cleaning and polishing. After polishing, a Nital2 solution was used for etching. Finally, the micrographs were analyzed with and without PWHT.

2.2. Microhardness test

A microhardness test was executed using a Shimadzu HMV-G30DT Vicker's microhardness tester. A relatively low Vickers Hardness (0.5 kg) was chosen to obtain the precise hardness in the

different locations: the MZ, the HAZ, and the BM. A microhardness test was executed with and without PWHT from the tool side to the operator side. For each sample, we conducted 21 microhardness tests with a dwell time of 15 s.

3. Results and discussion

A bainite microstructure was obtained when TIG welding was performed on a C67 material with PWHT in the MZ (Figure 1). As soon as welding was performed, the welded part of the material was heated by an electric heater at 710 ℃ for 99 s followed by air cooling at ambient temperature.

During continuous cooling, the cooling rate to form bainite is higher than that required to form pearlite, but slower to form martensite (in steels of the same composition). Most alloying elements will lower the temperature required for the maximum rate of formation of bainite, and carbon is the most effective among them [19]. Even though the microstructures of martensite and bainite at first seem quite similar, under a simple optical microscope, the microstructure of bainite appears darker than martensite due to its low reflectivity.

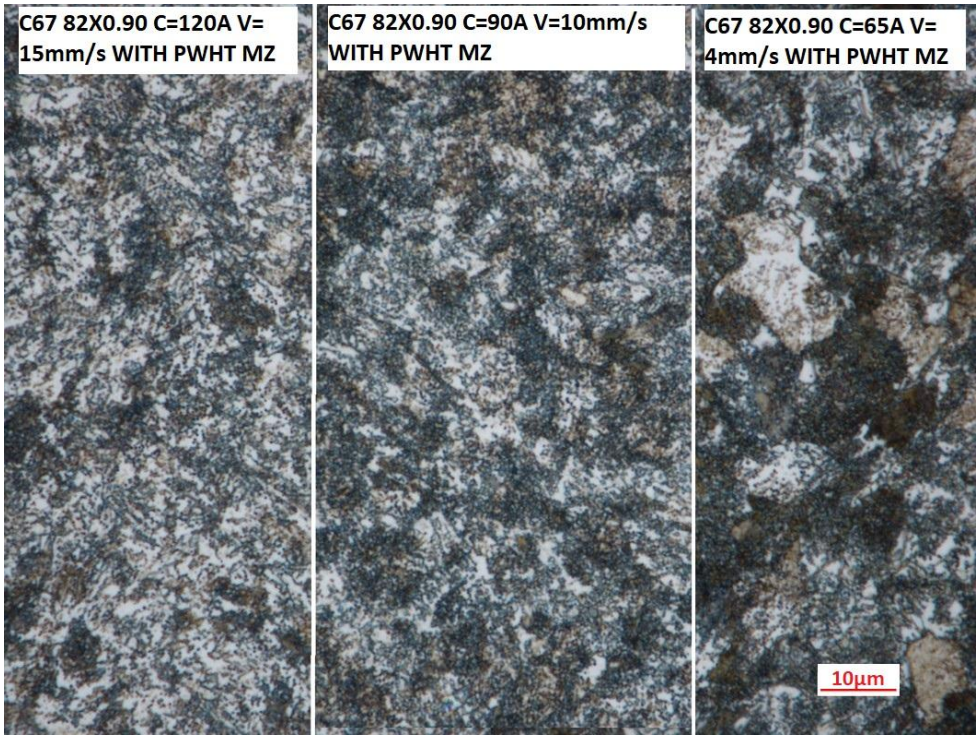

Figure 1. Melting zone area for different welding parameters with PWHT.

A relatively increased degree of hardness was observed on the tool side (Figure 2) of the welded part with PWHT for all welding parameters. Welding was initiated from the tool side and concluded on the operator side. The welding part on the tool side takes more time compared to operator side when the welding part is kept in the maintaining phase at 710 ℃ (i.e., the tool side started to cool while welding was continued on the operator side).

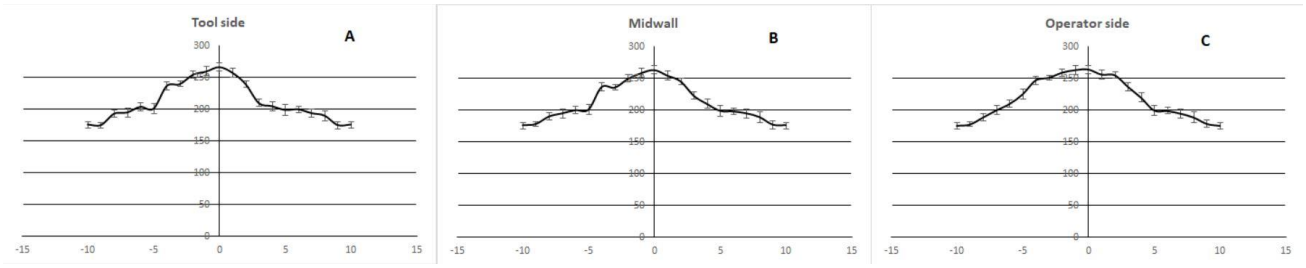

Figure 2. Hardness in tool, mid-wall and operator side. The welding was performed with PWHT.

As a result, the tool side rapidly cooled and developed an increased degree of hardness compared to the operator side. In our study, the highest degree of hardness measured in the tool side was 267 HV, while it measured 264 HV in the operator side of the MZ area. The hardness difference among the three zones is not statistically significant ($p < 0.05$). When the hardness was measured 10 mm from the center line of the MZ, the hardness was similar to the BM area and hardness was evenly distributed throughout the HAZ area.

The thermal diffusivity of the base material plays a vital role—if the diffusivity is high, the material cools fast and the HAZ is relatively small [22]; conversely, a low diffusivity leads to slower cooling and a larger HAZ. In addition, the amount of heat generated during welding is an important parameter to consider. For example, a processes like oxyfuel welding uses a high heat input which rises the size of the HAZ (Figure 3). A bainitic microstructure was formed in the MZ, while a mixer of globular and bainitic structures was evident in the HAZ. Moreover, processes like laser beam welding and electron beam welding give a highly concentrated, limited amount of heat, resulting in a small HAZ.

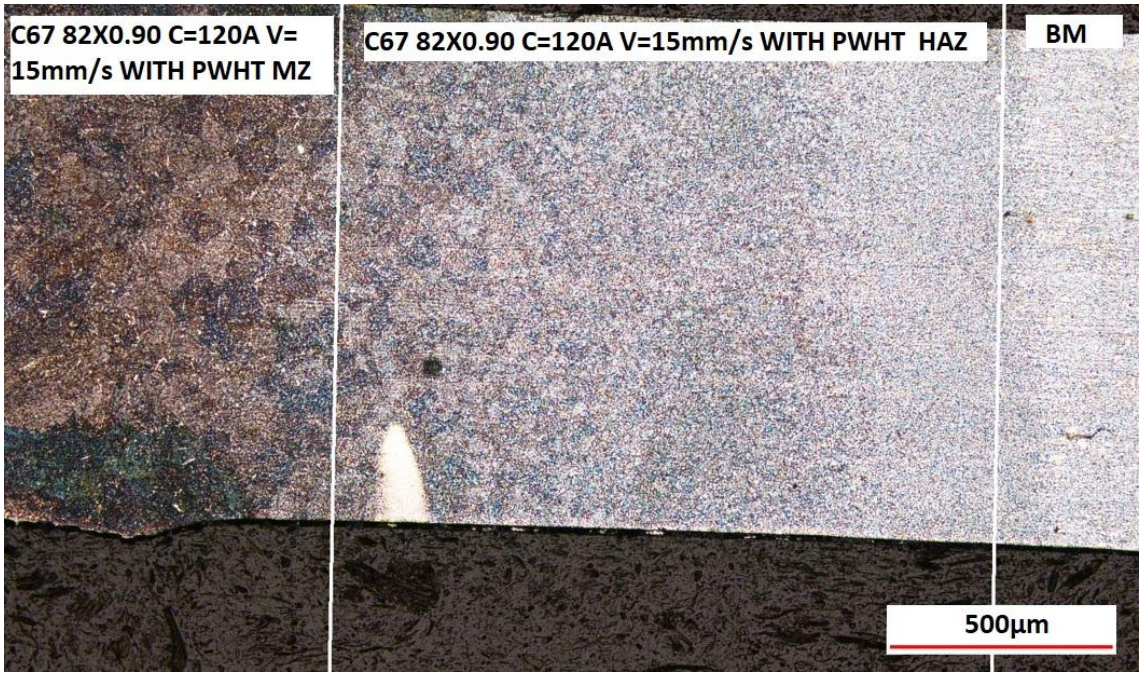

Figure 3. Base material, heat affected zone and melting zone in PWHT condition.

On the contrary, the HAZ without PWHT was relatively smaller in size (Figure 4) when compared to samples with PWHT. The heat spread out for a long area owing to slow cooling, while with PWHT, it cools quickly and does not have sufficient time to spread the heat.

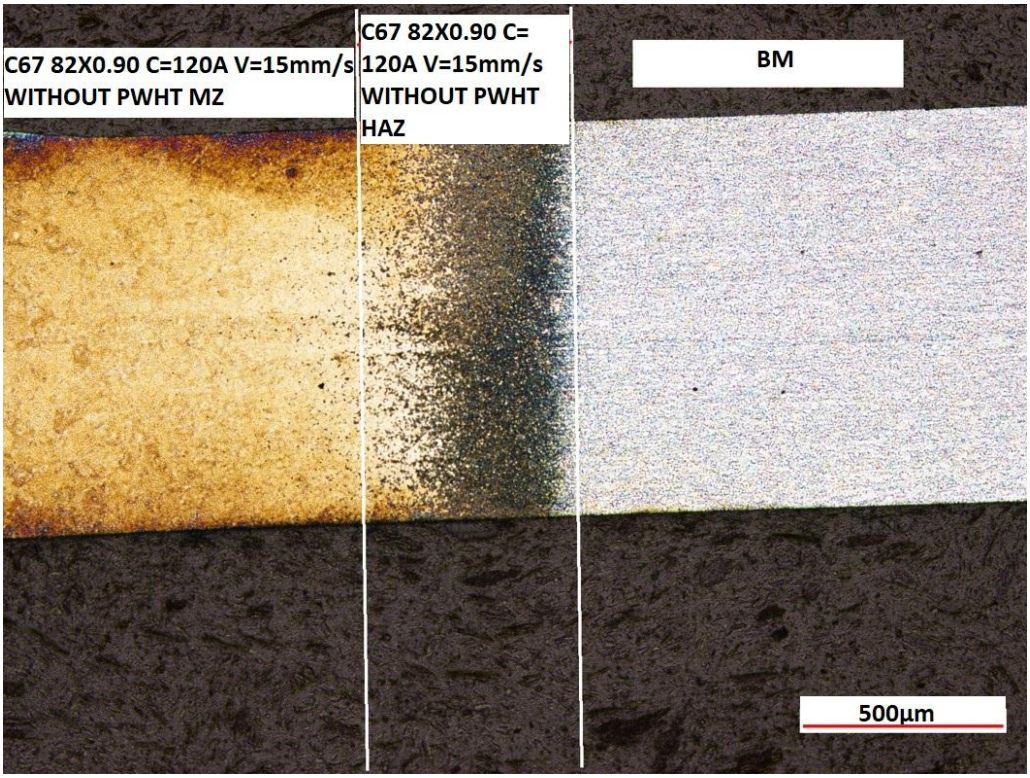

Figure 4. Base material, heat affected zone and melting zone when the welding was performed with the PWHT.

A martensitic microstructure is obtained by utilizing TIG welding on C67 material is done without post welding heat treatment (PWHT) in the MZ (Figure 5). The welding was performed above 1500 ℃ and the welded part was cooled to room temperature in air. The martensite is formed by rapid cooling (quenching) of austenite, which traps carbon atoms that do not have time to diffuse out of the crystal structure [38]. This martensitic reaction begins during cooling when the austenite reaches the martensite start temperature (MST) and the parent austenite becomes mechanically unstable. At a constant temperature below MST, a fraction of the parent austenite transforms rapidly, preventing any further transformations.

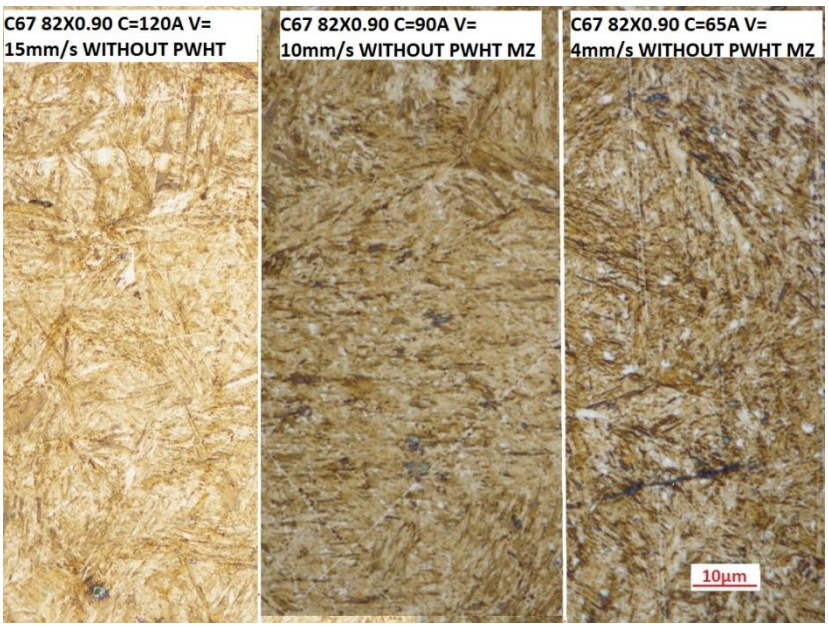

Figure 5. Melting Zone area when the welding was performed without PWHT.

As the temperature decreases, more of the austenite transforms to martensite, and eventually completes the transformation when the martensite finish temperature (MFT) is reached, generating a crack in the middle, particularly in the MZ area (Figure 6). This crack results from nonequilibrium cooling: thermodynamically metastable phase martensite is formed instead of stable phase where energy is released by crack formation. The microstructure of the HAZ and MZ are also similar to the welding sample without PWHT. Hence, the hardness of those two areas are not significantly different for all welding parameters.

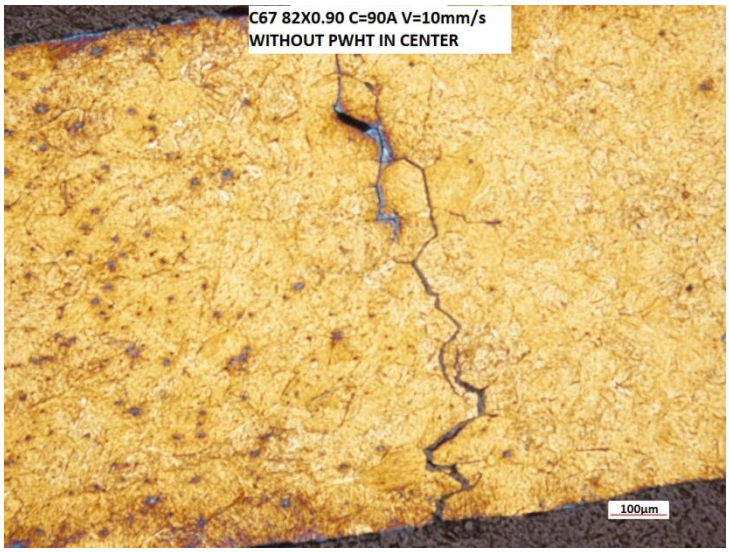

Figure 6. A crack was found in the melting zone area when the welding was performed without PWHT.

A martensitic microstructure is observed in the welding sample without PWHT, while bainite is developed with PWHT. In the HAZ, all parts of the material can't completely transform to martensite and the hardness of the HAZ area is relatively lower than melting zone area: the area of the HAZ is relatively higher in PWHT samples. Therefore, a sharp change of the hardness value is found in the HAZ compared to TIG done without PWHT (Figure 7). Overall, samples without PWHT possess relatively increased hardness values compared to PWHT due to martensite formation. The MZ area of the welding sample performed with PWHT is different from the welding sample performed without PWHT when the same parameters are used.

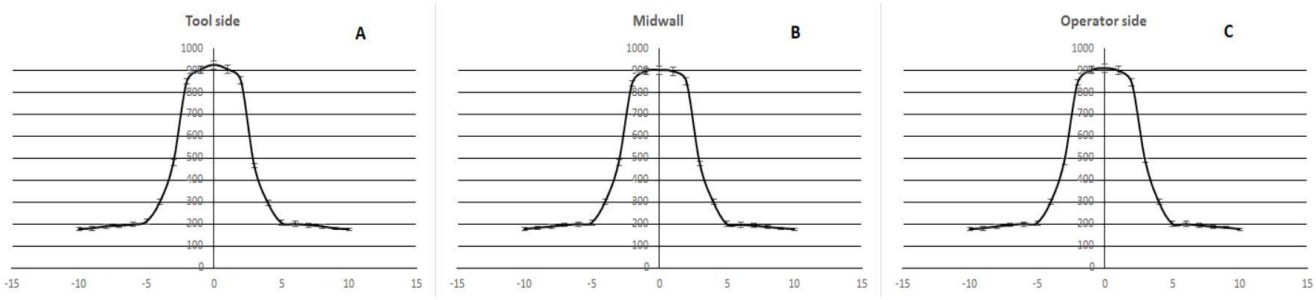

Figure 7. Hardness in tool, midwall and operator side. The welding was performed with PWHT.

A relatively high hardness is observed on the tool side (925 HV) compared with the operator side (910 HV) when a 100 A current with 7 mm/s velocity is used. The hardness measured 5mm from the center line of the MZ is similar with the BM area in this procedure. Moreover, a crack in the middle part was observed in samples without PWHT because of non-equilibrium cooling and the formation of meta-stable phase martensite.

In this study, hardness of the MZ and HAZ were insignificant when the welding was executed with PWHT. To obtain the minimum hardness in the MZ area, a 90 A current and 10 mm/s velocity were used, then the welded parts were kept at 710 ℃ for 99 s. A relatively higher magnitude of current was employed when the welding speed rose to avoid the welding spots [39]. Hence, a relatively higher welding speed (15 mm/s) was used where the 120 A current was applied. Moreover, a 265 HV hardness was detected on the MZ area where the hardness was distributed uniformly. Finally, we noticed a crack on the machine side where the welding was performed with a relatively low current and velocity (Figure 8).

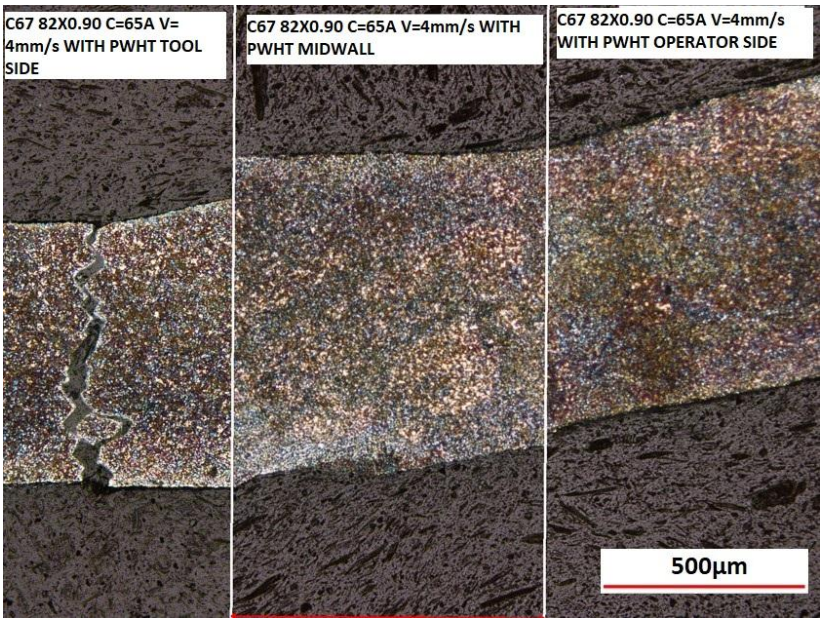

Figure 8. The welding section in tool's, midwall and operator side when the same parameters was used. The welding was performed with PWHT.

4. Conclusions

This work concentrates on the investigation of microstructure and mechanical properties of TIG welded on a C67 material considering its hardness by using different welding processing parameters. A higher hardness was noticed in the MZ area when TIG welding was performed without PWHT, and a sharp change of the hardness was observed in the HAZ area. The microhardness in the MZ zone was around 900 HV when the welding was executed without PWHT, and it was about 280 HV with PWHT. A crack in the middle part of the welded sample was noticed when the welding was performed without PWHT, as well as a sharp change of hardness. Furthermore, optical micrographs exhibited bainite formation in the MZ area when PWHT was performed, while a martensitic microstructure was developed when TIG welded was performed without PWHT. Overall, an increased degree of hardness was obtained in the welded samples without PWHT in either the MZ or HAZ. The microhardness was uniform on the tool side, mid-wall, and operator side for both procedures. The Vicker's hardness between the machine side and tool side was not statistically significant ($P < 0.005$). Though the microstructure was similar from the tool's side to the operator's side, a relatively higher hardness was detected in the tool's side, regardless of the application of PWHT. In this study, a larger HAZ area was seen when the welding was performed with PWHT. Finally, the lowest hardness was measured with a 90 A current and 10mm/s velocity was employed for welding, followed by PWHT and the hardness was 265 HV.

In the future, a laser welding can be performed on 0.90 mm of a C67 grade sheet to verify the microhardness and microstructure in the melting zone and compare it with the TIG welding. Our research didn't use any preheating on the samples before the welding, which could affect the grain size of the heat affected zone for welding with PWHT. Additionally, we can compare the grain size with preheating for both procedures.

Use of AI tools declaration

The authors declare they have not used Artificial Intelligence (AI) tools in the creation of this article.

Conflict of interest

There is no conflict of interest in writing and publishing the report.

References

1. Ayanoglu MO, Tauhiduzzaman M, Carlsson LA (2022) In-plane compression modulus and strength of Nomex honeycomb cores. *J Sandw Struct Mater* 24: 627–642. https://doi.org/10.1177/10996362211021888
2. Tauhiduzzaman M, Carlsson LA, Ayanoglu MO (2021) Design analysis of end notch flexure sandwich specimen with honeycomb core. *J Compos Mater* 55: 1295–1308. https://doi.org/10.1177/0021998320967050
3. İrsel G (2022) Study of the microstructure and mechanical property relationships of shielded metal arc and TIG welded S235JR steel joints. *Mater Sci Eng A-Struct* 830: 142320. https://doi.org/10.1016/j.msea.2021.142320
4. Wu X, Zhao X, Chen J, et al. (2022) Simulation of the influence of welding parameters on weld pool behavior during a TIG-MIG hybrid welding process. *J Manuf Process* 79:460–475. https://doi.org/10.1016/j.jmapro.2022.05.007
5. Pang S, Cao B (2021) Low current arc ignition stability in micro-TIG welding. *J Manuf Process* 69: 12–20. https://doi.org/10.1016/j.jmapro.2021.07.022
6. Zala AB, Jamnapara NI, Sasmal CS, et al. (2022) Study of microstructure & mechanical properties of TIG welded aluminized 9Cr-1Mo steel. *Fusion Eng Design* 176: 113038. https://doi.org/10.1016/j.fusengdes.2022.113038
7. Li T, Bi X, Li R (2022) A strategy for bonding immiscible Mg/steel by laser-TIG butt fusion welding and lattice distortion on the Fe/Mg interface matching. *Mater Design* 219:110763. https://doi.org/10.1016/j.matdes.2022.110763
8. Pydi HP, Pasupulla AP, Vijayakumar S, et al. (2021) Study on microstructure, behavior and Al_2O_3 content flux A-TIG weldment of SS-316L steel. *Mater Today Proc* 51: 728–734. https://doi.org/10.1016/j.matpr.2021.06.218
9. Panda SS (2021) Characterisation of Cu–Al alloy lap joint using TIG Welding. *CIRP J Manuf Sci Technol* 35: 454–459. https://doi.org/10.1016/j.cirpj.2021.07.009
10. Mahajan A, Singh H, Kumar S, et al. (2022) Mechanical properties assessment of TIG welded SS 304 joints. *Mater Today Proc* 56:3073–3077. https://doi.org/10.1016/j.matpr.2021.12.133
11. Nguyen VN, Nguyen QM, Huang SC (2018) Microstructure and mechanical properties of butt joints between stainless steel sus304l and aluminum alloy A6061-T6 by TIG welding. *Materials* 11: 1136. https://doi.org/10.3390/ma11071136
12. Anwar S, Rehman AU, Usmani Y, et al. (2021) Influence of post weld heat treatment on the grain size, and mechanical properties of the alloy-800h rotary friction weld joints. *Materials* 14: 4366. https://doi.org/10.3390/ma14164366

13. Li D, Lu S, Dong W, et al. (2012) Study of the law between the weld pool shape variations with the welding parameters under two TIG processes. *J Mater Process Technol* 212: 128–136. https://doi.org/10.1016/j.jmatprotec.2011.08.015
14. Zmitrowicz P, Kawiak M, Kochmański P, et al. (2021) Microstructure and mechanical properties of welded joints of 1.4462 duplex steel made by the k-tig method. *Materials* 14: 7868. https://doi.org/10.3390/ma14247868
15. Li M, Yao D, Guan Y, et al. (2020) Effect of welding speed and post quenching on the microstructure and mechanical properties of laser-welded B1500HS joints. *Materials* 13: 4645. https://doi.org/10.3390/ma13204645
16. Fei Z, Pan Z, Cuiuri D, et al. (2019) Microstructural characterization and mechanical properties of K-TIG welded SAF2205/AISI316L dissimilar joint. *J Manuf Process* 45: 340–355. https://doi.org/10.1016/j.jmapro.2019.07.017
17. Konat Ł (2021) Technological, microstructural and strength aspects of welding and post-weld heat treatment of martensitic, wear-resistant hardox 600 steel. *Materials* 14: 4541. https://doi.org/10.3390/ma14164541
18. Alipooramirabad H, Paradowska A, Nafisi S, et al. (2020) Post-weld heat treatment of api 5l x70 high strength low alloy steel welds. *Materials* 13: 5801. https://doi.org/10.3390/ma13245801
19. Królicka A, Radwański K, Janik A, et al. (2020) Metallurgical characterization of welded joint of nanostructured bainite: Regeneration technique versus post welding heat treatment. *Materials* 13: 4841. https://doi.org/10.3390/ma13214841
20. Chaudry UM, Ahmad HW, Tariq MR, et al. (2020) Effect of post weld heat treatment on the microstructure and electrochemical characteristics of dissimilar material welded by butter method. *Materials* 13: 4512. https://doi.org/10.3390/ma13204512
21. Tian S, Xu F, Zhang G, et al. (2021) Influence of post-weld heat treatment on microstructure and toughness properties of 13MnNiMoR high strength low alloy steel weld joint. *Materials* 14: 5336. https://doi.org/10.3390/ma14185336
22. Brykov MN, Petryshynets I, Džupon M, et al. (2020) Microstructure and properties of heat affected zone in high-carbon steel after welding with fast cooling in water. *Materials* 13: 5059. https://doi.org/10.3390/ma13225059
23. Smith M, Bichler L, Gholipour J, et al. (2017) Mechanical properties and microstructural evolution of in-service Inconel 718 superalloy repaired by linear friction welding. *Int J Adv Manuf Tech* 90: 1931–1946. https://doi.org/10.1007/s00170-016-9515-2
24. Drabble DJ, Bishop CM, Kral M (2011) A microstructural study of grain boundary engineered alloy 800H. In: Metallurgical and Materials Transactions A: Physical Metallurgy and Materials Science. pp 763–772
25. Wang H, Ikeuchi K, Aritoshi M, et al. (2009) Microstructures forming in friction welding of Inconel 718 alloy—joint performance and its controlling factors in friction welding of Inconel 718 alloy. *Weld Int* 23: 670–678. https://doi.org/10.1080/09507110902842869
26. Szczucka-Lasota B, Węgrzyn T, Szymczak T, et al. (2021) High martensitic steel after welding with micro-jet cooling in microstructural and mechanical investigations. *Materials* 14: 936. https://doi.org/10.3390/ma14040936

27. Lan L, Shao G (2020) Morphological evolution of HAZ microstructures in low carbon steel during simulated welding thermal cycle. *Micron* 131: 102828. https://doi.org/10.1016/j.micron.2020.102828
28. Sehgal AK (2020) An investigation of variable welding current on impact strength of metal inert gas welded specimen. *Mater Today Proc* 37: 3679–3682. https://doi.org/10.1016/j.matpr.2020.10.151
29. Pham CH, Trinh HN, Proust G (2021) Effect of manufacturing process on microstructures and mechanical properties, and design of cold-formed G450 steel channels. *Thin Wall Struct* 162: 107620. https://doi.org/10.1016/j.tws.2021.107620
30. Bodude MA, Momohjimoh I (2015) Studies on effects of welding parameters on the mechanical properties of welded low-carbon steel. *J Miner Mater Char Eng* 3: 142–153. https://doi.org/10.4236/jmmce.2015.33017
31. Bansal A, Kumar MS, Shekhar I, et al. (2021) Effect of welding parameter on mechanical properties of TIG welded AA6061. *Mater Today Proc* 37: 2126–2131. https://doi.org/10.1016/j.matpr.2020.07.567
32. Boumerzoug Z, Derfouf C, Baudin T (2010) Effect of welding on microstructure and mechanical properties of an industrial low carbon steel. *Engineering* 2: 502–506. https://doi.org/10.4236/eng.2010.27066
33. Shrivas SP, Vaidya SK, Khandelwal AK, et al. (2019) Investigation of TIG welding parameters to improve strength. *Mater Today Proc* 26: 1897–1902. https://doi.org/10.1016/j.matpr.2020.02.416
34. Su L, Fei Z, Davis B, et al. (2021) Digital image correlation study on tensile properties of high strength quenched and tempered steel weld joints prepared by K-TIG and GMAW. *Mater Sci Eng A-Struct* 827: 142033. https://doi.org/10.1016/j.msea.2021.142033
35. Fei Z, Pan Z, Cuiuri D, et al. (2019) Improving the weld microstructure and material properties of K TIG welded armour steel joint using filler material. *Int J Adv Manuf Technol* 100: 1931–1944. https://doi.org/10.1007/s00170-018-2787-y
36. Fei Z, Pan Z, Cuiuri D, et al. (2019) Effect of heat input on weld formation and tensile properties in keyhole mode TIG welding process. *Metals* 9: 1327. https://doi.org/10.3390/met9121327
37. Kumar K, Kumar CS, Masanta M, et al. (2021) A review on TIG welding technology variants and its effect on weld geometry. *Mater Today Proc* 50: 999–1004. https://doi.org/10.1016/j.matpr.2021.07.308
38. Li Y, Guan Q, He B (2023) Improving the strength and ductility of medium Mn steel by depleting the stress-assisted martensite. *Scr Mater* 226: 115267. https://doi.org/10.1016/j.scriptamat.2022.115267
39. Cui S, Pang S, Pang D, et al. (2021) Influence of welding speeds on the morphology, mechanical properties, and microstructure of 2205 DSS welded joint by k-tigwelding. *Materials* 14: 3426. https://doi.org/10.3390/ma14123426